Experimental Mechanics (2018) 58:1249–1263
https://doi.org/10.1007/s11340-018-0411-6

Evaluation of Conformal and Non-Conformal Contact Parameters Using Digital Photoelasticity

M.P. Hariprasad[1] · K. Ramesh[2] · B.C. Prabhune[2]

Received: 22 November 2017 / Accepted: 12 June 2018 / Published online: 25 June 2018
© Society for Experimental Mechanics 2018

Abstract
Experimental studies to exploit photoelastic data of conformal geometries to extract contact parameters are non-existent because closed-form stress field equations were not available until recently. In this paper, the explicit equations recently reported in the literature for a flat punch with rounded edges are generalized so that a single set of equations can be used for a flat punch with rounded edges and Hertzian contacts with arbitrary radii of curvatures. The generality of the governing equations is verified by plotting isochromatics for conformal and non-conformal contact situations. A generic method to evaluate unknown contact parameters from the whole-field isochromatic data for conformal and non-conformal geometries is implemented. The methodology is initially verified using theoretically generated isochromatic data and is then used to experimentally evaluate two contact situations. In view of high-fringe gradient zones, the suitability of various digital photoelastic methods is compared. A novel four-step phase shifting technique is proposed in which isochromatic and isoclinic data can be evaluated using the minimum number of images.

Keywords Contact mechanics · Flat rounded punch · Muskhelishvili potential · Digital photoelasticity · Phase shifting technique

Introduction

In many mechanical devices, contact between two or more parts exists and is crucial in the load transfer from one component to another. Although analytical modeling of contact zones has received attention [1–6], reports of whole-field equations for stress fields are limited. For non-conformal contacts, Smith and Liu [5] in 1953 derived stress field equations in terms of the contact length and frictional coefficient. Contact problems involving conformal geometries, such as a flat punch with a rounded edge, are more complex since a combination of complete and incomplete contact zones can be produced [1, 2]. Although the subsurface stress fields can be formulated based on the Muskhelishvili complex potential approach [3], most work focuses on obtaining pertinent information on only the contacting interface or along the line of symmetry [2, 4, 6]. Experimental studies to exploit photoelastic data of conformal geometries to extract contact parameters are non-existent since closed-form stress field equations have not been available until recently. Only in 2014, Jesus Vazquez et al. [7] reported the stress fields for a flat punch with rounded edge contact.

In this paper, the explicit equations reported in the literature for a flat punch with rounded edges are generalized so a single set of equations can be used for a flat punch with rounded edges and Hertzian contacts with arbitrary radii of curvatures by considering the relative curvature term. To obtain insight into the contact of a flat punch with rounded edges, theoretically simulated isochromatics and isoclinics are obtained by varying the friction between the bodies in contact. With the modified explicit stress field equations, a generic methodology is implemented to determine contact stress parameters for conformal and non-conformal geometries from the whole-field experimental isochromatic data using a nonlinear least squares approach. The methodology is initially verified using analytically simulated contact fields and then applied to two examples of conformal and non-conformal contact problems. In view of high-fringe gradient zones, the suitability of various digital photoelastic methods is compared, and an improved four-step Phase Shifting Technique (PST) is proposed to evaluate isochromatic and isoclinic data using a minimum number of images.

✉ K. Ramesh
kramesh@iitm.ac.in

M. P. Hariprasad
hprasadmp@gmail.com

[1] Department of Mechanical Engineering, Amrita Vishwa Vidyapeetham, Amritapuri, India

[2] Department of Applied Mechanics, Indian Institute of Technology Madras, Chennai 600036, India

Sub-Surface Stress Fields for Contact Zones

Muskhelishvili Potential in terms of arbitrarily distributed normal $p(s)$ and tangential load $q(s)$ for the contact problem is given as [2, 3].

$$\Phi(z) = \frac{1}{2\pi i}\int_{contact}\frac{p(s)-iq(s)}{s-z}ds \tag{1}$$

where $z = x + iy$ and s is the measure of distance along the contacting interface in the x-direction from the origin (Fig. 1(a)). Stress components are related to Muskhelishvili potential ($\Phi(z)$) as

$$\begin{aligned}\sigma_{xx}+\sigma_{yy} &= 2\left(\Phi(z)+\overline{\Phi(z)}\right)\\ \sigma_{yy}-\sigma_{xx}+2i\tau_{xy} &= 2\left(\bar{z}\Phi'(z)+\Psi(z)\right)\end{aligned} \tag{2}$$

where $\Psi(z) = -\Phi(z)-\overline{\Phi(\bar{z})}-z\Phi'(z)$. Here, the over bar sign indicates the complex conjugate, and the dash indicates the derivative of the complex variable.

Failure or yielding according to von Mises criteria can be obtained as $\Phi(z)$a function of Muskhelishvili Potential and its derivatives as

$$\sigma_{vM}^2 = \begin{cases}\gamma_1^2+3\delta_1\bar{\delta}_1, & \text{for plane stress}\\ (1-2\nu)^2\gamma_1^2+3\delta_1\bar{\delta}_1, & \text{for plane strain}\end{cases} \tag{3}$$

where

$$\begin{aligned}\gamma_1 &= (1/2)(\sigma_x+\sigma_y) = \left(\Phi(z)+\overline{\Phi(z)}\right)\\ \delta_1 &= (1/2)(\sigma_y-\sigma_x+2i\tau_{xy}) = \left(\bar{z}\Phi'(z)-\Phi(z)-\overline{\Phi\left(\bar{z}\right)}-z\Phi'(z)\right)\end{aligned} \tag{4}$$

Since this could be evaluated directly using equation (2), separation of the individual stress components (σ_{xx}, σ_{yy}, τ_{xy}) is not necessary, and explicit equations were not reported for conformal contacts until recently.

For conformal contacts, the classic rigid punch is simple to evaluate but not realistic. Civerella et al. [6] and Sackfield et al. [4] studied the influence of the corner radius of a flat punch using a complex potential approach, thereby providing a realistic alternative to the classic rigid-flat punch idealization. Extending the work of Civerella et al. [6] and Sackfield et al. [4], Jesus Vazquez et al. [7] obtained the explicit solutions in the real domain for the stress field for a flat punch with rounded edge contact (Fig. 1). When external load is applied, the flat region $-b$ to b is in complete contact, and the segments b to a and $-b$ to $-a$ are in incomplete contact.

The Muskhelishvili Potential for normal (Φ^n) and tangential load (Φ^t) for generic loading is expressed as

$$\Phi^n(z) = \begin{cases}\dfrac{i(z+b)\Delta}{2C}+\Delta\dfrac{i\sqrt{z^2-a^2}\left(\pi-2\sin^{-1}(k)\right)-(z-b)\ln(\Omega(z,b))+(z+b)\ln(\Omega(z,-b))}{2C\pi}, & x\le 0\\ \dfrac{i(z-b)}{2C}+\Delta\dfrac{-i\sqrt{z^2-a^2}\left(\pi-2\sin^{-1}(k)\right)-(z-b)\ln(-\Omega(z,b))+(z+b)\ln(-\Omega(z,-b))}{2C\pi}, & x>0\end{cases} \tag{5}$$

$$\Phi^t(z) = \begin{cases}\dfrac{-\mu(z+b)\Delta}{2C}+i\mu\Delta\dfrac{\sqrt{z^2-a^2}\left(\pi-2\sin^{-1}(k)\right)-(z-b)\ln(\Omega(z,b))+(z+b)\ln(\Omega(z,-b))}{2C\pi}, & x\le 0\\ \dfrac{-\mu(z-b)\Delta}{2C}+i\mu\Delta\dfrac{\sqrt{z^2-a^2}\left(\pi-2\sin^{-1}(k)\right)-(z-b)\ln(-\Omega(z,b))+(z+b)\ln(-\Omega(z,-b))}{2C\pi}, & x>0\end{cases} \tag{6}$$

where k is the ratio of the two contact lengths b/a (Fig. 1), C is a measure of compliance of the bodies in contact and Δ is the relative curvature defined as

$$\Delta = \left(\frac{1}{R_1}+\frac{1}{R_2}\right) \tag{7}$$

where R_1 and R_2 are the radii of the curvature of the contacting bodies. For similar bodies, the measure of compliance (C) is defined as $C = (\kappa+1)/(2G)$, where G is the shear modulus and κ is Kolosov's constant, which is $\kappa = (3-\nu)/(1+\nu)$ for plane stress and $\kappa = (3-4\nu)$ for plane strain situations with ν being Poisson's ratio. The symbol Ω in equations (5) and (6) is defined as

$$\Omega(z,t) = \frac{\sqrt{\dfrac{z-a}{z+a}}-i\sqrt{\dfrac{a-t}{a+t}}}{\sqrt{\dfrac{z-a}{z+a}}+i\sqrt{\dfrac{a-t}{a+t}}} \tag{8}$$

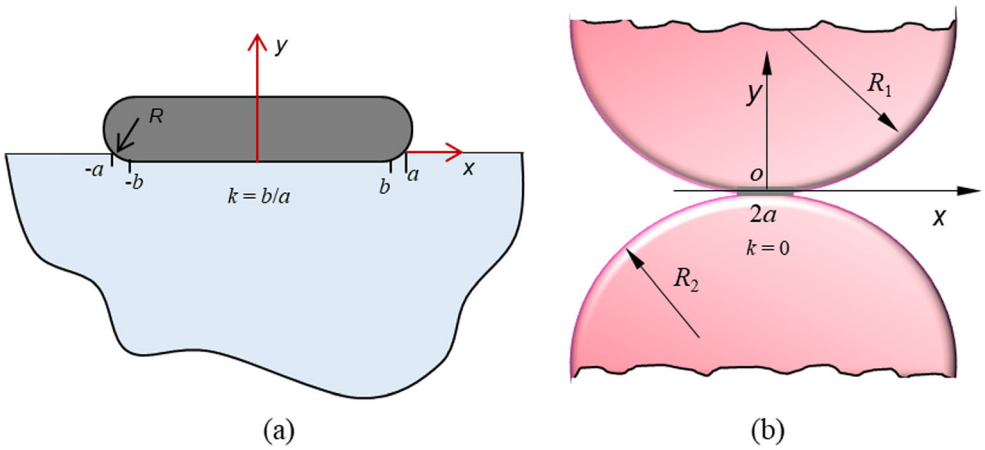

Fig. 1 Schematic diagram of contact zone of (a) flat punch with rounded edge and (b) two discs

For a flat punch with a rounded edge, the pressure term can be obtained in dimensionless form as [6]

$$p(\omega)=\frac{P}{b}\frac{-2/\pi}{\pi-2\omega_0-\sin 2\omega_0}\left\{(\pi-2\omega_0)\cos\omega+\ln\left[\left|\frac{\sin(\omega+\omega_0)}{\sin(\omega-\omega_0)}\right|^{\sin\omega}\left|\tan\frac{\omega+\omega_0}{2}\tan\frac{\omega-\omega_0}{2}\right|^{\sin\omega_0}\right]\right\} \tag{9}$$

where

$$\omega=\sin^{-1}\left(\frac{x\sin\omega_0}{b}\right)\text{ and }\omega_0=\sin^{-1}(b/a)$$

A generalized explicit solution of the normal and tangential stress component (superscripts 'n' and 't') for conformal and non-conformal geometries with varying radii of curvature of the contacting bodies is expressed as

$$\sigma^n_{xx}(x,y)=\begin{cases}\dfrac{-2y\Delta}{C}-\Delta\dfrac{(v_1+yu_6)\left(\pi-2\sin^{-1}(k)+2y(v_3-v_2)-(b+x)u_3+(x-b)u_2\right)}{C\pi}, & x\le 0\\ \dfrac{-2y\Delta}{C}-\Delta\dfrac{(-v_1-yu_6)\left(\pi-2\sin^{-1}(k)+2y(v_3-v_2)-(b+x)u_3+(x-b)u_2\right)}{C\pi}, & x>0\end{cases} \tag{10}$$

$$\sigma^n_{yy}(x,y)=\begin{cases}-\Delta\dfrac{(v_1-yu_6)\left(\pi-2\sin^{-1}(k)\right)-(b+x)u_3+(x-b)u_2}{C\pi}, & x\le 0\\ -\Delta\dfrac{(-v_1+yu_6)\left(\pi-2\sin^{-1}(k)\right)-(b+x)u_3+(x-b)u_2}{C\pi}, & x>0\end{cases} \tag{11}$$

$$\sigma^n_{xy}(x,y)=\begin{cases}-\Delta\dfrac{y\left(v_6\left(2\sin^{-1}(k)-\pi\right)+u_3-u_2\right)}{C\pi}, & x\le 0\\ -\Delta\dfrac{y\left(v_6\left(\pi-2\sin^{-1}(k)\right)+u_3-u_2\right)}{C\pi}, & x>0\end{cases} \tag{12}$$

$$\sigma^t_{xx}(x,y)=\begin{cases}-\mu\Delta\dfrac{(2u_1-yv_6)\left(\pi-2\sin^{-1}(k)+3y(u_3-u_2)+2(b+x)(v_3+\pi)-2(x-b)v_2\right)}{C\pi}, & x\le 0\\ -\mu\Delta\dfrac{(-2u_1+yv_6)\left(\pi-2\sin^{-1}(k)+3y(u_3-u_2)+2(b+x)(v_3+\pi)-2(x-b)v_2\right)}{C\pi}, & x>0\end{cases} \tag{13}$$

$$\sigma^t_{yy}(x,y)=\begin{cases}-\Delta\dfrac{(v_1-yu_6)\left(\pi-2\sin^{-1}(k)\right)-(b+x)u_3+(x-b)u_2}{C\pi}, & x\le 0\\ -\Delta\dfrac{(-v_1+yu_6)\left(\pi-2\sin^{-1}(k)\right)-(b+x)u_3+(x-b)u_2}{C\pi}, & x>0\end{cases} \tag{14}$$

$$\sigma^t_{xy}(x,y)=\begin{cases}-\mu\Delta\dfrac{(v_1+yu_6)\left(\pi-2\sin^{-1}(k)+2y(v_3-v_2-\pi)+(b+x)u_3-(x-b)u_2\right)}{C\pi}, & x\le 0\\ -\mu\Delta\dfrac{(-v_1-yu_6)\left(\pi-2\sin^{-1}(k)+2y(v_3-v_2)-(b+x)u_3+(x-b)u_2\right)}{C\pi}, & x>0\end{cases} \tag{15}$$

Parameters u_1, u_2, u_3, u_6, v_1, and v_6 used in equations (10)–(15) are functions of x, y, a and b and are defined in Appendix 1.

For combined loading conditions, which are prevalent in most practical applications, the stress components can be obtained through the linear superposition of normal and tangential components as

$$\sigma_{ij}(x,y) = \sigma_{ij}^{n}(x,y) + \sigma_{ij}^{t}(x,y) \tag{16}$$

For a punch with a rounded edge contacting a base plate with an infinite radius of curvature (Fig. 1), Δ has a value of $(1/R)$, where R is the radius of the punch and the set of equations (equations (10)–(16)) takes the form reported in Ref. [7]. For an incomplete contact length $b = 0$, i.e., $k = 0$, this takes a contact interface of two discs such as the Hertzian case (Fig. 1(b)), where a is defined as semi-contact length and $2a$ is the total contact length with appropriate values for Δ depending on the curvatures of the contacting bodies. A simple modification of introducing a relative curvature term of the contacting bodies (Δ) extends the equations for a flat punch with rounded edge contact [7] to model a Hertzian contact field with any arbitrary radius of curvature of the contacting bodies.

Verification of Generalized Governing Equations by Plotting Isochromatics for Contact Zones

The principal stress difference (σ_1 - σ_2) in the entire domain can be easily obtained using equations (10)–(16). The isochromatic fringe field for the contact zone can be simulated using the Stress- Optic law as

$$I_d = 255\sin^2\left(\frac{t(\sigma_1-\sigma_2)}{2\pi F_\sigma}\right) \tag{17}$$

where I_d is the intensity value of the dark field isochromatics, t is the thickness of the model (mm) and F_σ is the material stress fringe value (N/mm/fringe). Equation (17) converts the retardation information into an 8-bit grayscale representation, where the intensity value 255 represents pure white and 0 represents pitch black.

In equations (10)–(16), if k is equal to zero, the solution is the Hertzian solution. Figure 2(a) shows typical isochromatics for Hertzian contacts. Figure 2(b) shows the variation in the fringe order at $x = 0$ along y/a for different values of k with $\Delta = 1/R$. For k values other than zero, it simulates various combinations of a flat punch with rounded edges. Figure 2(c) shows the simulated isochromatic fringes for $k = 0.4$, which splits the eye of the Hertzian contact and pulls the maximum fringe order zones towards the ends of the punch.

Nature of Isochromatic and Isoclinic Fringe Fields for Flat Punch with Rounded Edges

To show the equations model a flat punch with rounded edges, a sample problem with $R = 2$ mm, $b = 3$ mm, $E = 3.3$ GPa, $\nu = 0.37$, and $k = 0.96$ is theoretically generated with and without friction ($\mu = 1.5$, 0). The principal stress data obtained are plotted as dark field isochromatics (Figs. 3(a) and 3(b)). Figure 3(c) shows the fringe order variation along a line at $y = -0.1a$ for different frictional coefficients, $\mu = 0$, 0.1, 0.15, 0.2, and 0.3. From Fig. 3(c), the additional tangential traction induced on the contacting surface increases the level of fringe orders with increased frictional coefficients.

The isoclinic fringe fields provide information on the orientation of principal stress throughout the model domain. The isoclinics should be plotted over the domain as binary contours of 10° steps to mimic the assembly of isoclinic contours as seen in a conventional photoelastic experiment. The isoclinic data obtained for $\mu = 0$, and 0.15 is plotted as binary contours and shown in Figs. 4(a) and 4(b). From Figs. 4(a) and 4(b), the isoclinics are symmetric with respect to the vertical axis in the absence of friction. However, the presence of tangential traction disturbs the symmetrical distribution of isoclinics. Variation in the isoclinic data along a line at $y = -0.1a$ for different frictional coefficients, $\mu = 0$, 0.1, 0.15, 0.2, and 0.3, is plotted in Fig. 4(c). From Fig. 4(c), the effect of additional tangential traction induced on the contacting surface on isoclinic data is mainly in the region of $-1 < x/a < 1$, i.e., along the contact length.

Evaluation of Contact Stress Field Parameters from Isochromatic Fringe Field

Formulation of Nonlinear Least Squares

In this section, the methodology to determine the unknown contact parameters from the whole-field isochromatics is described. The fringe order N and principal stress difference $(\sigma_1 - \sigma_2)$ are related by the stress-optic law as [8, 9].

$$\sigma_1 - \sigma_2 = \frac{NF_\sigma}{t} \tag{18}$$

where t is the thickness of the model (mm) and F_σ is the material stress fringe value. Substituting the principal stress difference calculated from equations (10)–(16) into equation (18), an error function g is defined for the n^{th} data point as

$$g_n(a,b,\mu) = \left((\sigma_1-\sigma_2) - \frac{N^{\exp}F_\sigma}{t}\right)_n \tag{19}$$

Through equations (10)–(16), it is noted that the expression for (σ_1- σ_2) is non-linear in terms of total contact lengths (a, b)

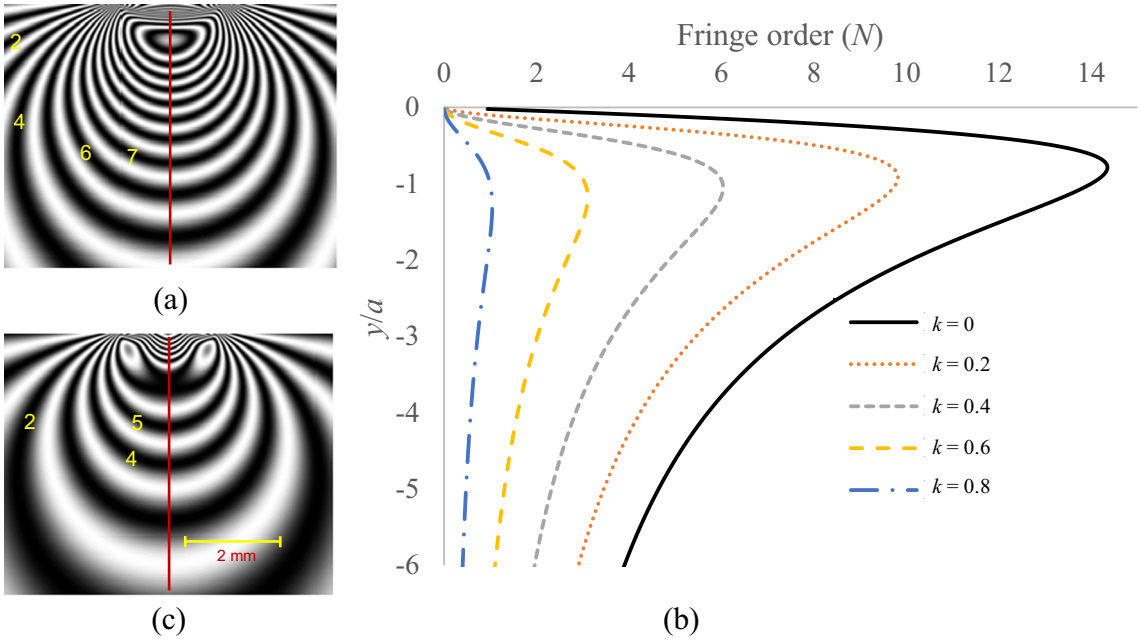

Fig. 2 (a) Theoretically generated isochromatics of the contact zone for $k = 0$. (b) Variation in the fringe order at $x = 0$ for different k values ($a = 1$ mm, $R = 20$ mm). (c) Theoretically generated isochromatics of the contact zone for $k = 0.4$

Fig. 3 Theoretically generated isochromatics for flat punch with rounded edge ($R = 2$ mm, $b = 3$ mm, $k = 0.96$, $\nu = 0.37$) for (a) frictionless and (b) friction coefficient $\mu = 0.1$. (c) Fringe order variation along a line at $y = -0.1a$ for different frictional coefficients

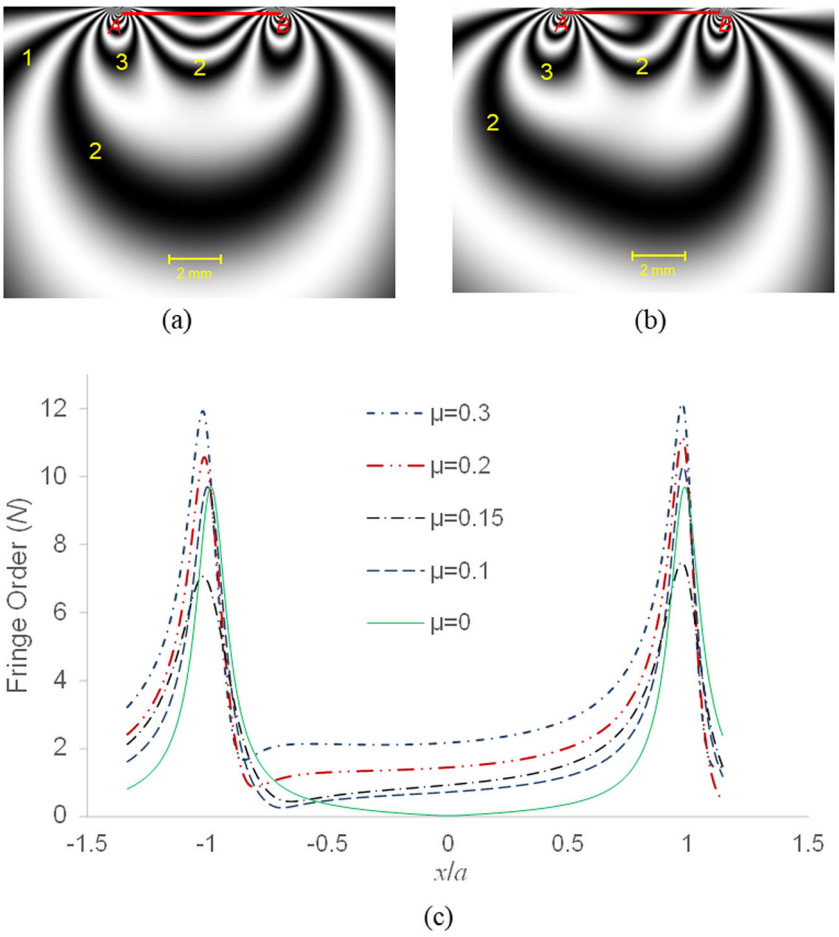

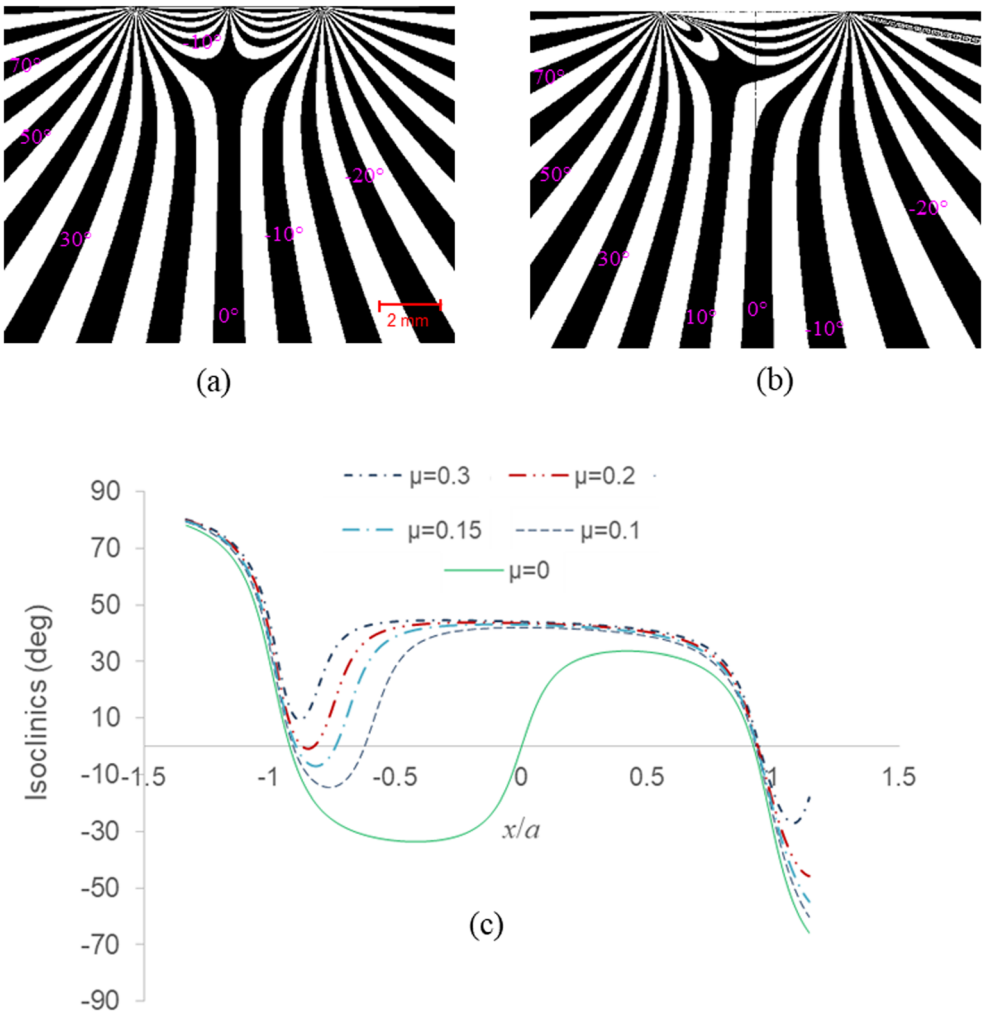

Fig. 4 Binary representation of theoretically generated isoclinics for flat punch with rounded edge ($R = 2$ mm, $b = 3$ mm, $k = 0.96$, $\nu = 0.37$) for (a) frictionless and (b) friction coefficient $\mu = 0.15$. (c) variation in isoclinic data along a line at $y = -0.1a$ for different frictional coefficients

and the frictional coefficient μ. Based on Taylor series expansion, the error function can be expressed in terms of g and its correction factor for the parameters (Δa, Δb, $\Delta\mu$) for the i^{th} iteration as

$$-(g_n)_i = \left(\frac{\partial g_n}{\partial a}\right)_i (\Delta a)_i + \left(\frac{\partial g_n}{\partial b_x}\right)_i (\Delta b)_i + \left(\frac{\partial g_n}{\partial \mu}\right)_i (\Delta\mu)_i \qquad (20)$$

Applying equation (20) to n data points can be represented in matrix form as

$$\begin{Bmatrix} g_1 \\ g_2 \\ \vdots \\ g_n \end{Bmatrix}_i = -\begin{bmatrix} \frac{\partial g_1}{\partial a} & \frac{\partial g_1}{\partial b} & \frac{\partial g_1}{\partial \mu} \\ \frac{\partial g_2}{\partial a} & \frac{\partial g_2}{\partial b} & \frac{\partial g_2}{\partial \mu} \\ \vdots & \vdots & \vdots \\ \frac{\partial g_n}{\partial a} & \frac{\partial g_n}{\partial b} & \frac{\partial g_n}{\partial \mu} \end{bmatrix}_i \begin{Bmatrix} \Delta a \\ \Delta b \\ \Delta\mu \end{Bmatrix}_i \qquad (21)$$

Following ref. [8], this set of equations is solved in an over-deterministic approach and the parameters are modified in the $i+1$th iteration using (Δa, Δb, $\Delta\mu$). Iteration is stopped using fringe order minimization criteria. In fringe order minimization, the fringe orders corresponding to the selected data points are calculated theoretically for every iteration and compared with the experimental fringe orders. This iteration is stopped using the convergence criterion:

$$\frac{\sum |N_{\text{theory}} - N_{\text{exp}}|}{\text{no.of data points}} \leq \text{convergence error} \qquad (22)$$

Initially, the correctness of this methodology is verified using the theoretically generated data shown in Figs. 3(a) and (b). In photoelastic data analysis of crack problems, collecting data on fringe contours has been shown to provide improved results [10]. Following this, the fringe order data and corresponding positional coordinates are obtained along the fringe contours. The results from the least squares algorithm for Fig. 4(a) ($a = 3.151$ mm, $k = 0.96$, $\mu = 3.9 \times 10^{-6}$, Convergence error $= 8.07 \times 10^{-6}$) and for Fig. 4(b) ($a = 3.149$ mm, $k = 0.96$, $\mu = 0.149$, Convergence error $= 6.3 \times 10^{-6}$) are in good agreement with the parameters used for theoretical generation, which indicates the correctness of the implemented procedure. The contact zones are reconstructed using the results obtained from the least squares analysis with the data echoed back and

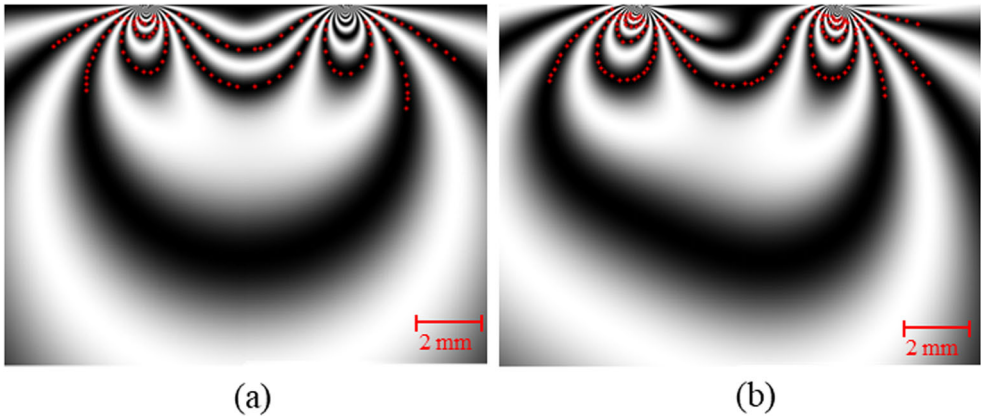

Fig. 5 Reconstructed isochromatics and data points echoed back using contact parameters obtained from the nonlinear least squares result for the contact shown in (a) Fig. 3(a) and (b) Fig. 3(b)

are shown in Figs. 5(a) and (b). A convergence error value less than 0.1 generally produces good solutions.

Experimental Evaluation of Whole-Field Isochromatics of Contact Zones

Different digital photoelastic methods are explored for data extraction, and a brief summary of the methods is provided.

Whole-Field Isochromatic and Isoclinic Evaluation of Contact Zones Using Phase Shifting

Recent developments in digital photoelasticity have allowed evaluating the isochromatics and isoclinic parameters over the entire model domain with considerable accuracy [11, 12]. Among the different phase shifting algorithms [12], the ten-step phase shifting method proposed by Ramji and Ramesh [13] provides photoelastic parameters with the highest accuracy [9, 12]. The optical configurations for the ten-step PST are given in Table 1. The first four configurations (1 to 4) correspond to a plane polariscope [14, 15] (Fig. 6(a)), and the next six configurations (5 to 10) correspond to a circular polariscope [16, 17] (Fig. 6(b)). In the intensity expressions, I_a and I_b represent the amplitude of light and background light intensity, respectively. Phase retardation and the principal stress direction in the model are represented by δ and θ. The orientations of the polarizer and analyzer axes with respect to the horizontal axis are referred to as α and β. The orientations of the slow axis of the first and second quarter wave plates are indicated by ξ and η, respectively.

From the first four phase-shifted images, the whole-field Isoclinic parameter can be obtained using

$$\theta_c = \frac{1}{4}\tan^{-1}\left(\frac{(I_{4,R}+I_{4,G}+I_{4,B})-(I_{2,R}+I_{2,G}+I_{2,B})}{(I_{3,R}+I_{3,G}+I_{3,B})-(I_{1,R}+I_{1,G}+I_{1,B})}\right) \quad (23)$$

where subscript 'c' indicates the principal value of the inverse trigonometric function and is calculated using the 'atan2()' function. Subscripts R, G, and B refer to the Red, Green and Blue color planes of the image. Isoclinic values obtained using equation (23) are in wrapped format, i.e., they are in the range of $-\pi/4$ to $\pi/4$, whereas physically, θ is in the range of $-\pi/2$ to $\pi/2$. The wrapped isoclinics are unwrapped using an adaptive quality guided algorithm [13].

Table 1 Optical arrangement for ten-step PST and corresponding intensity equations

α	ξ	η	β	Intensity Equation
$\pi/2$	–	–	0	$I_1 = I_b + I_a \sin^2\frac{\delta}{2}\sin^2 2\theta$
$5\pi/8$	–	–	$\pi/8$	$I_2 = I_b + \frac{I_a}{2}\sin^2\frac{I_a}{2}[1-\sin 4\theta]$
$3\pi/4$	–	–	$\pi/4$	$I_3 = I_b + I_a \sin^2\frac{\delta}{2}\cos^2 2\theta$
$7\pi/8$	–	–	$3\pi/8$	$I_4 = I_b + \frac{I_a}{2}\sin^2\frac{I_a}{2}[1+\sin 4\theta]$
$\pi/2$	$3\pi/4$	$\pi/4$	$\pi/2$	$I_5 = I_b + \frac{I_a}{2}(1+\cos\delta)$
$\pi/2$	$3\pi/4$	$\pi/4$	0	$I_6 = I_b + \frac{I_a}{2}(1-\cos\delta)$
$\pi/2$	$3\pi/4$	0	0	$I_7 = I_b + \frac{I_a}{2}(1-\sin 2\theta\sin\delta)$
$\pi/2$	$3\pi/4$	$\pi/4$	$\pi/4$	$I_8 = I_b + \frac{I_a}{2}(1+\cos 2\theta\sin\delta)$
$\pi/2$	$\pi/4$	0	0	$I_9 = I_b + \frac{I_a}{2}(1+\sin 2\theta\sin\delta)$
$\pi/2$	$\pi/4$	$3\pi/4$	$\pi/4$	$I_{10} = I_b + \frac{I_a}{2}(1-\cos 2\theta\sin\delta)$

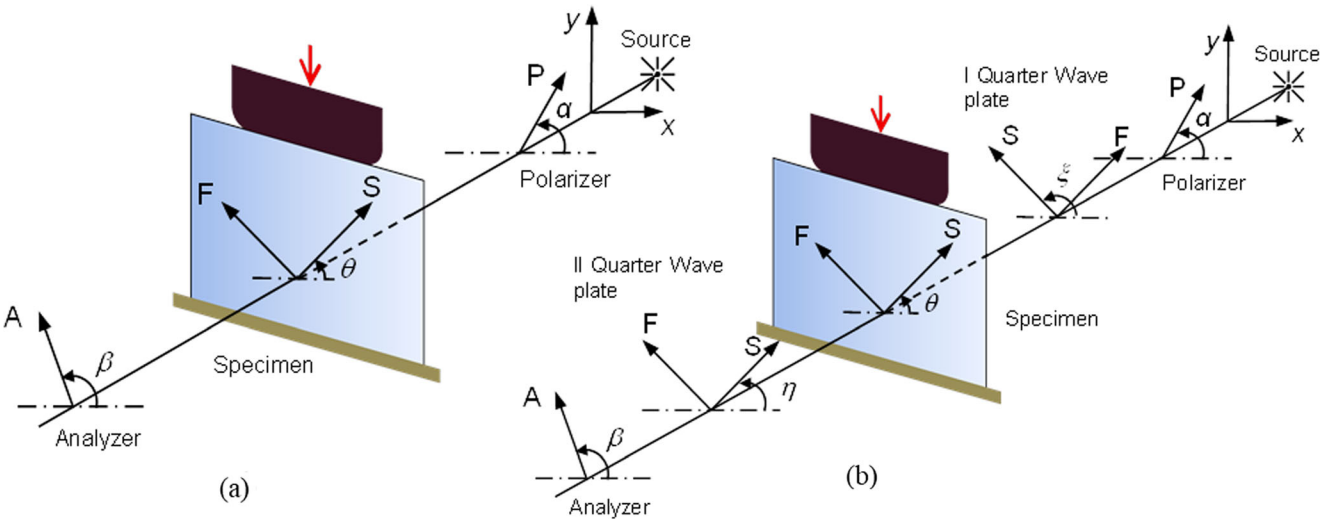

Fig. 6 Generic optical configurations: (a) circular polariscope and (b) plane polariscope

From the corresponding phase-shifted images, the isochromatic information can be obtained using the relation

$$\delta_c = \tan^{-1}\left(\frac{(I_9-I_7)\sin 2\theta + (I_8-I_{10})\cos 2\theta}{(I_5-I_6)}\right) \tag{24}$$

Monochromatic illumination is preferred for isochromatic evaluation using Equation (24). This requires an image acquisition system with the same pixel resolutions in the color and monochromatic domains, which is difficult in many experimental situations. To circumvent this issue, the phase-shifted images can be acquired in the color domain, the three channels (Red, Blue and Green) can be used for isoclinic evaluation, and the green channel can be used to process the isochromatic information using equation (24) [18].

The ten-step method advocates using an unwrapped theta (θ) for evaluating delta information using equation (24), which results in an ambiguous-free wrapped isochromatic phase map. The fringe order evaluated using equation (24) is also in wrapped form, which is subsequently unwrapped to obtain the total fringe order in the entire model domain.

Isochromatic Evaluation by twelve Fringe Photoelasticity

In Twelve Fringe Photoelasticity (TFP), only one image is recorded, and the total fringe order is evaluated by comparing the color components of the experimental isochromatics with those in the calibration table using a color difference formula, which is given as

$$e = \sqrt{(R_m-R_c)^2 + (G_m-G_c)^2 + (B_m-B_c)^2 + (H_m-H_c)^2 + (S_m-S_c)^2 + (V_m-V_c)^2} \tag{25}$$

where subscript 'm' refers to the experimentally obtained intensity values for a data point in the model and 'c' denotes the values in the calibration table. Subscripts *R, G, and B* and *H, S, and V* refer to the *Red, Green, and Blue* color planes and the *Hue, Saturation, and Value* of a pixel in the image, respectively.

Equation (25) may lead to a false estimation of fringe orders in some regions of the model due to the repetition of colors. This noise is removed by imposing fringe order continuity using a modified window search method given as

$$e = \sqrt{(R_m-R_c)^2 + (G_m-G_c)^2 + (B_m-B_c)^2 + (H_m-H_c)^2 + (S_m-S_c)^2 + (V_m-V_c)^2} \quad N\in[N_p-\Delta N, N_p+\Delta N] \tag{26}$$

where $\Delta N = 0.4$. The average value of the fringe order of all neighboring resolved pixels is used as Np in equation (26). Equation (26) is employed using an improved scanning scheme called Fringe Resolution-based scanning for Twelve Fringe Photoelasticity (FRSTFP) [19], where the progression is guided by the spatial resolution of the isochromatic fringes.

Improved Four-Step Phase Shifting Technique in TFP

In the four-step phase shifting technique, four isoclinic images of 0°, 22.5°, 45° and 67.5° are recorded (first four arrangements of Table 1). It is worth noting that the dark field isochromatics can be generated by post-processing the isoclinic images. The intensities of the

Red, Green and Blue color planes of the isochromatics can be obtained using the relation [14]

$$IR_{cp} = \sqrt{\left(I_3^{cp} - I_1^{cp}\right)^2 + \left(I_4^{cp} - I_2^{cp}\right)^2} \quad (27)$$

Here, 'cp' refers to the image planes of the Red, Green and Blue color space. The fringe orders can be evaluated using TFP (equations (25), (26) and isoclinics by equation (23).

Experimental Methodology

Photoelastic experiments with different contact situations have been designed to verify the concepts discussed in Sections "Sub-

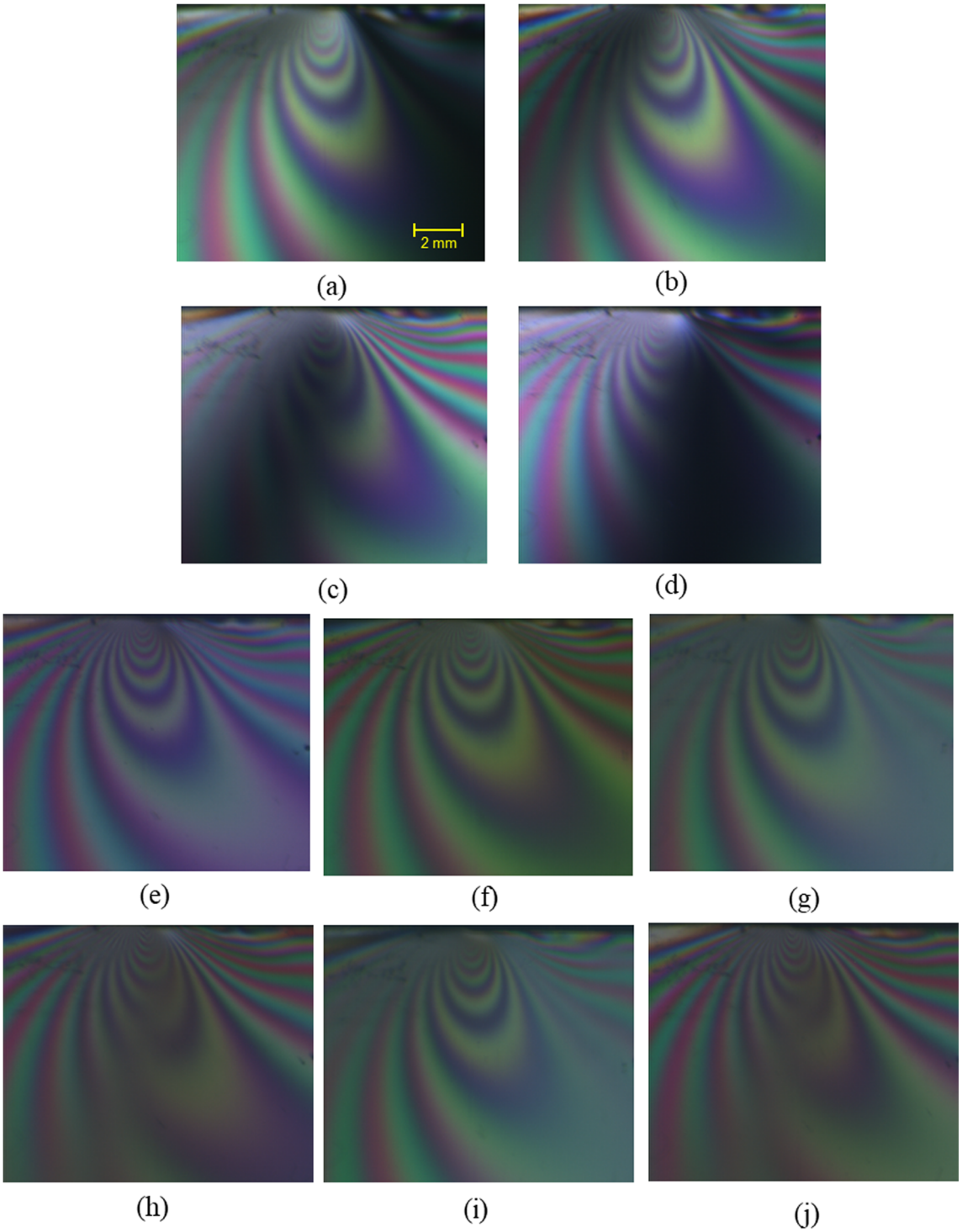

Fig. 7 Magnified view of the left side of the plate – punch with rounded edge interface. Ten-step phase shifting images according to Table 1 (a) – (j)

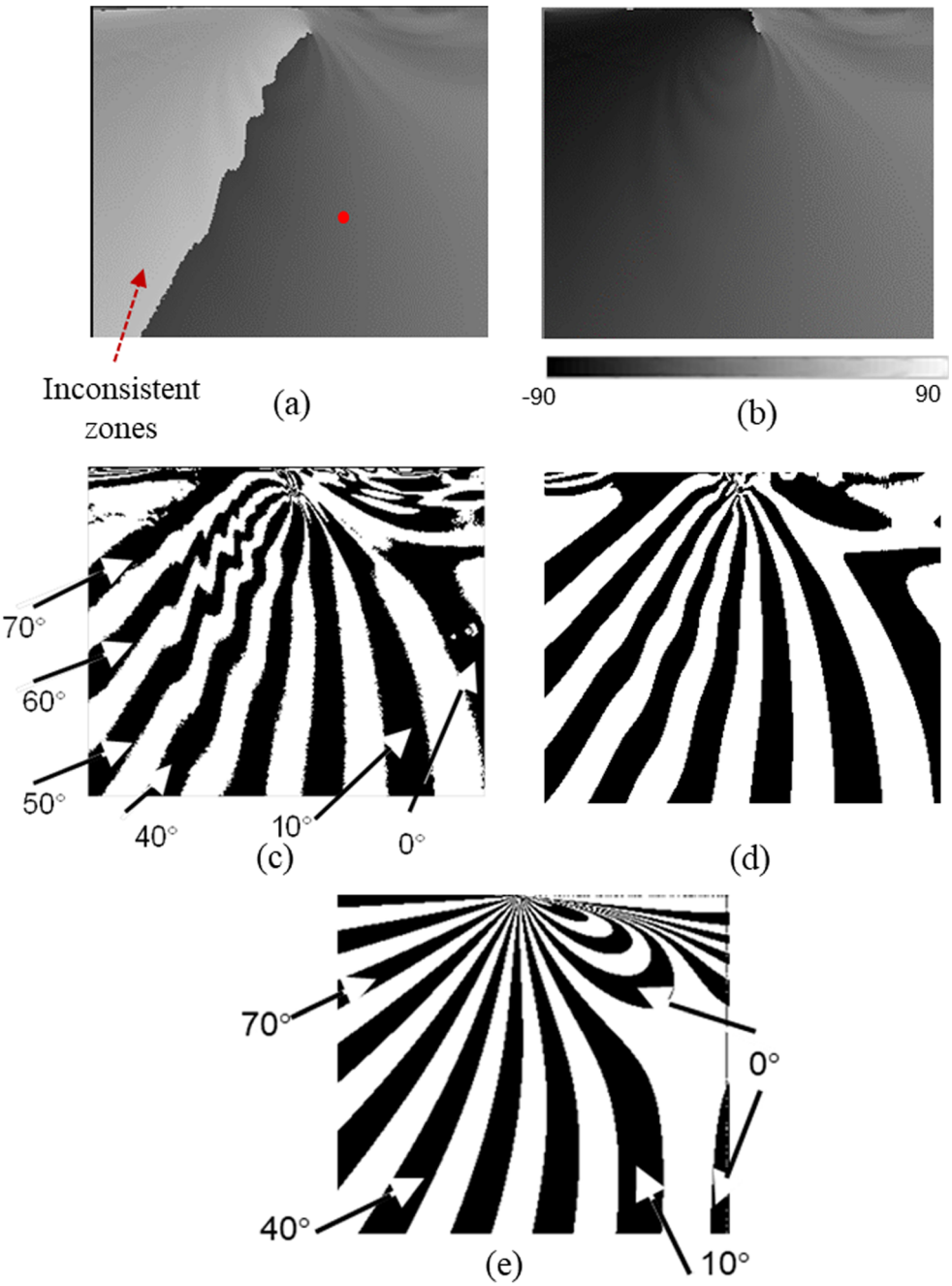

Fig. 8 Plate-Punch with rounded edge interface. (a) Wrapped isoclinic phasemap with seed point used for unwrapping. (b) Unwrapped isoclinic phasemap. Binary representation of isoclinic phasemap in 10° steps. (c) Unsmoothed. (d) Smoothed using multi-directional algorithm with a scanning sequence of 0°, 45°, 135°, 90°. (e) Theoretically simulated

Surface Stress Fields for Contact Zones" and "Evaluation of Contact Stress Field Parameters from Isochromatic Fringe Field". Experimental models are built using photoelastically sensitive material by mixing CY230 resin and HY951 hardener in a 10:1 ratio by weight. Two contact zones of conformal and non-conformal types are obtained by suitably changing the models. Initially, a flat punch with a rounded edge of a length of 11 mm and edge radius of 2 mm contacts a flat base plate with a length of 100 mm and a width of 40 mm. Next, a disc contacts another disc with the same radius ($R = 30$ mm). A loading fixture is designed and fabricated to apply compressive loading to the disc/punch. To investigate the isoclinic and isochromatic information in the conformal contacts, the ten-step experimental phase-shifted images as per the optical arrangement specified in Table 1 are recorded using a color 3CCD camera (SonyXC-003P) (Fig. 7(a)–(j)). Images are taken so the high-fringe gradient zone towards the contact region is captured.

Evaluation of experimental isochromatics using PST

In ten-step PST, isoclinics are calculated in the first step as discussed in Sec. "Whole-Field Isochromatic and Isoclinic Evaluation of Contact Zones Using Phase Shifting". Wrapped isoclinic phasemap obtained using equation (23) is shown in

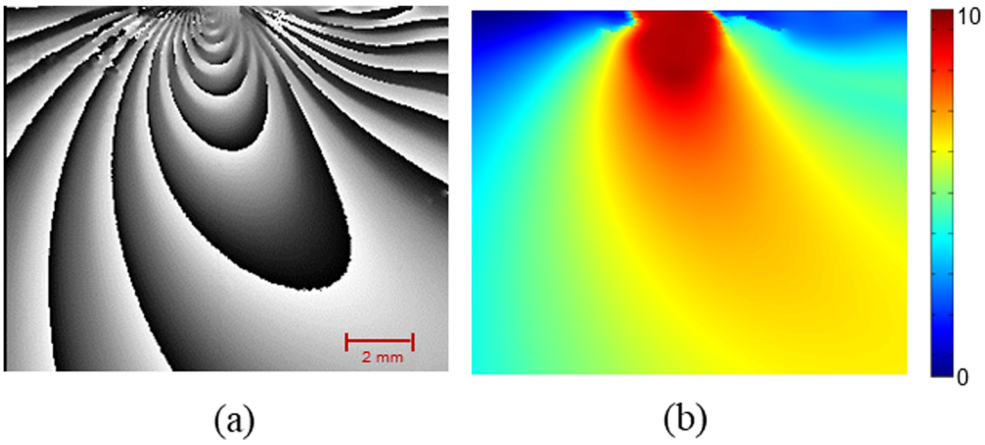

Fig. 9 Plate-Punch with rounded edge; (a) Wrapped isochromatics. (b) Whole-field plot of unwrapped isochromatics after smoothing

Fig. 8(a). Unwrapping is performed using a single-seed point, shown in Fig. 8(a), and the unwrapped isoclinics are shown as a phasemap in Fig. 8(b). A binary representation of isoclinics in steps of 10° is shown in Fig. 8(c). The noise in the isoclinics is clearly visible and is reduced using the multi-directional smoothing algorithm [20] in which smoothed data from a scan are used as the input for subsequent scans. A scanning sequence of 0°, 45°, 135°, and 90° with a span length of 15 pixels for 0° and 90° scans and 20 pixels for 135° and 45° is effective for removing noise from the isoclinic data. A binary representation of smoothed isoclinic data is shown in Fig. 8(d), which compares well with the theoretical isoclinic data shown in Fig. 8(e).

Using the unwrapped value of isoclinics in equation (24), phasemap of wrapped isochromatics is obtained and shown in Fig. 9 (a). This phasemap is unwrapped to obtain the total fringe order. Whole-field fringe order data after multi-directional smoothing with a scanning sequence of 90°, 135°, 45°, and 0° is shown as a whole-field plot in Fig. 9(b).

The problem of two discs in contact (Fig. 10(a)) (diameter = 60 mm, $\Delta = 2/R$, load = 316 N and $F_\sigma = 12.16$ N/mm/fringe) is also analyzed using the ten-step PST as explained in Sec. "Whole-Field Isochromatic and Isoclinic Evaluation of Contact Zones Using Phase Shifting". Dark-field isochromatics of a magnified portion of the contact region is shown in Fig. 10(b) and phaseshifted images are processed using ten-step PST. Unwrapped fringe order variation after multi-directional smoothing with a scanning sequence of 135°, 90°, 45°, and 0° and a span of 5 pixels is shown as a whole-field plot in Fig. 10(c).

Evaluation of experimental isochromatics using TFP

In this section, fringe order evaluation by TFP from circular polariscope-based dark field isochromatics and from the improved four-step method is compared with PST. From the recorded plane polariscope images (Figs. 7(a) – (d)), dark field isochromatics are generated using equation (27) and shown in Fig. 11(a). The fringe order obtained using equation (25) for generated isochromatics is shown in Figs. 11(b). Abrupt discontinuities in the fringe order data is refined using equation (26) with FRSTFP and the smoothed result with a scanning sequence of 0°, 45°, 135°, and 90° and a span length of 15

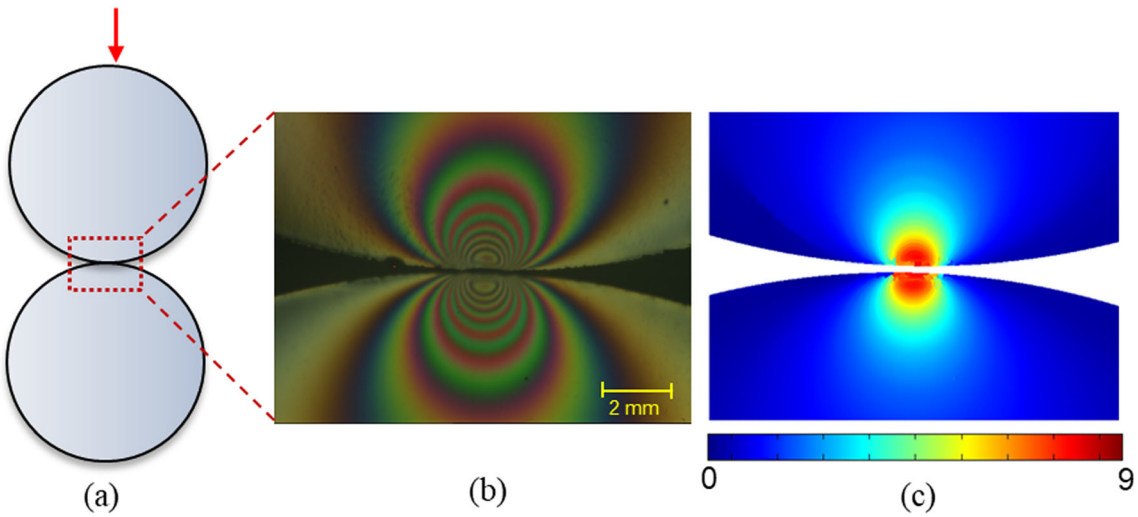

Fig. 10 Interface of two discs: (a) Schematic diagram. (b) Dark field isochromatics. (c) Whole-field plot of total fringe order obtained using PST

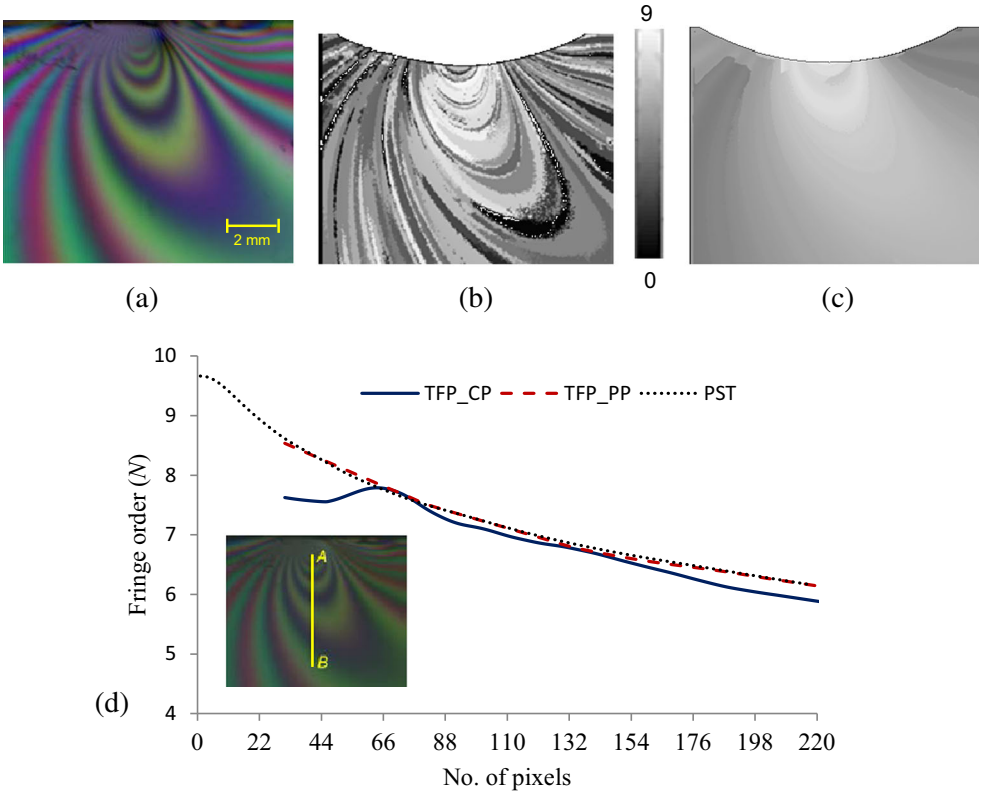

Fig. 11 (a) Generated dark field isochromatics of Plate–Punch with rounded edge interface from plane polariscope using equation (27). (b) Isochromatics in grayscale obtained using TFP from equation (26). (c) Refined fringe order in grayscale. (d) Variation of fringe order along line *AB* obtained from TFP Circular Polariscope (TFP-CP), Plane Polariscope (TFP-PP) and PST

pixels are shown in Fig. 11(c). Since processing involves refining and smoothing, isochromatic regions where the fringes are smudged are masked (Figs. 11(b) and (c)) and not considered in the processing to minimize noise propagation from such zones. A similar process is used to evaluate the fringe orders using Fig. 7(f). A comparison of the fringe order data obtained using TFP from a conventional circular polariscope dark field image (TFP_CP) and from the improved four-step method (TFP_PP) with PST data along line *AB* is shown in Fig. 11(d). The comparison of fringe orders from the improved four-step PST is quite good and can yield fringe orders up to 8.6. There are minor deviations in the fringe order results from processing the dark field circular polariscope image with a standard deviation of 0.23 fringe orders and fringe orders only up to 7.8 were yielded. Note that if the maximum fringe order to be processed is less than 3, TFP and the improved four-step method yield identical results [21]. Note that the isochromatics generated using equation (27) eliminate the quarter-wave plate mismatch errors since they are purely based on a plane polariscope algorithm.

The results obtained using TFP for the circular polariscope and improved four-step method yielded correct variations with maximum fringe orders of 7.8 and 8.6 for TFP_CP and TFP_PP, respectively, where the spatial resolution of the fringes is greater than 15 pixels per fringe. Hence, if the objective is to obtain information of both the isoclinics and isochromatics, the four-step PST proposed in Sec. "Improved Four-Step Phase Shifting Technique in TFP" can be used, and equations (27) and (23) can be used to obtain the fringe order and isoclinic results. If the objective is only fringe order evaluation, a single conventional isochromatic color image with TFP analysis would be sufficient. However, if there are constraints in the image acquisition system for obtaining high fringe resolutions (minimum of 15 pixels per fringe) in the key regions, PST is preferable.

Evaluation of Contact Parameters from Experimental Isochromatic Data

In this section, the whole-field fringe order data obtained from different digital photoelastic methods are utilized to determine unknown contact parameters for two different contacting interfaces. The fringe order data from PST and corresponding positional coordinates along the fringe contours are processed.

For a plate-punch interface contact, the contact parameter a is 5.72 mm with $k = 0.958$ and $\mu = 0.075$. This indicates the complete contact length closely matches the dimensions of the flat region of the punch. The unknown incomplete contact length due to the edge radius is 0.24 mm for this case. The isochromatics in the contact zone are reconstructed with the results obtained from the least squares analysis, and the data used for the analysis are echoed back on the reconstructed image (Fig. 12(a)). A whole-field error plot between the experimental

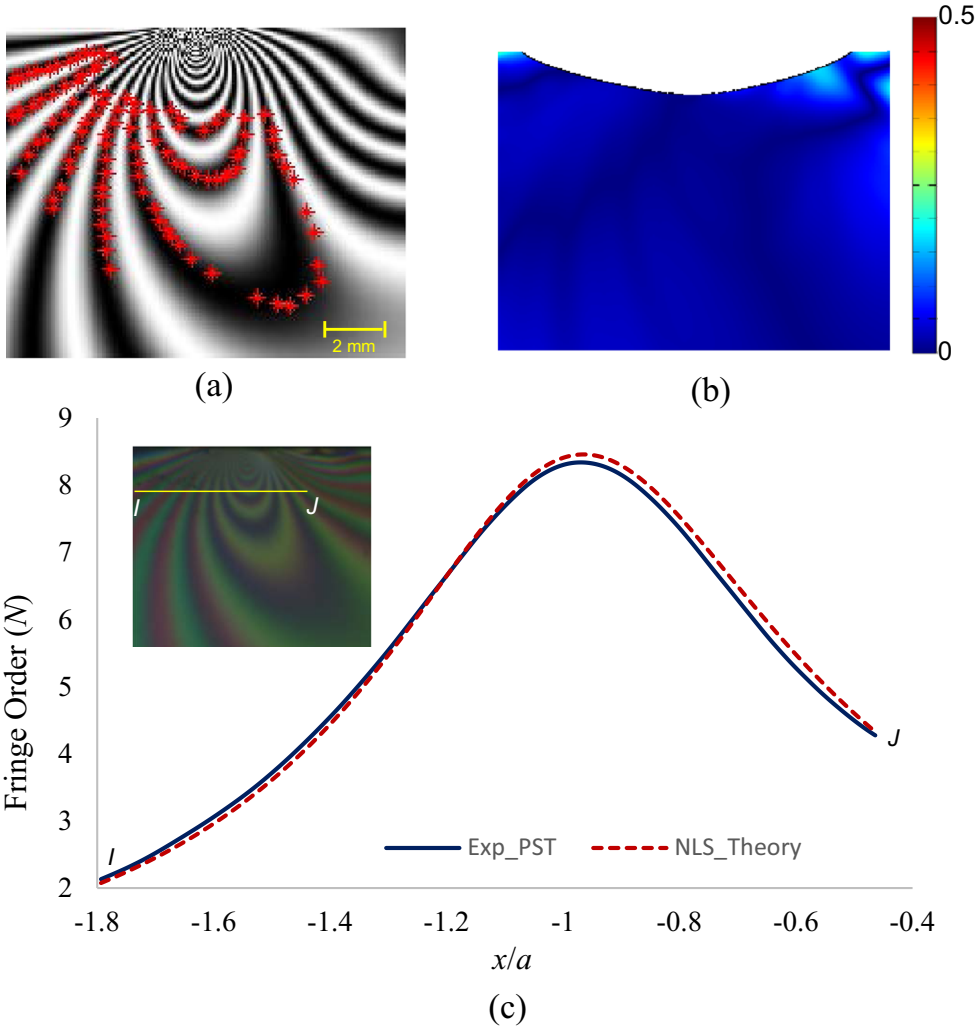

Fig. 12 Plate-Punch Interface – (a) Reconstructed isochromatics using the least squares results with data points echoed back for parameters obtained from PST. (b) Whole-field error plot of fringe order between PST and least squares. (c) Variation in the fringe order along line *IJ* for PST and reconstructed from least squares

and contact model using a least squares procedure is shown as a contour plot in Fig. 12(b). From Fig. 12(b), it is clear that other than localized zones where the fringes are smudged, the error in fringe orders range from 0.02 to 0.03. The variation in the fringe orders along line $y = 0.4a$ (line - *IJ*) from PST and the reconstructed contact zone is plotted in Fig. 12(c).

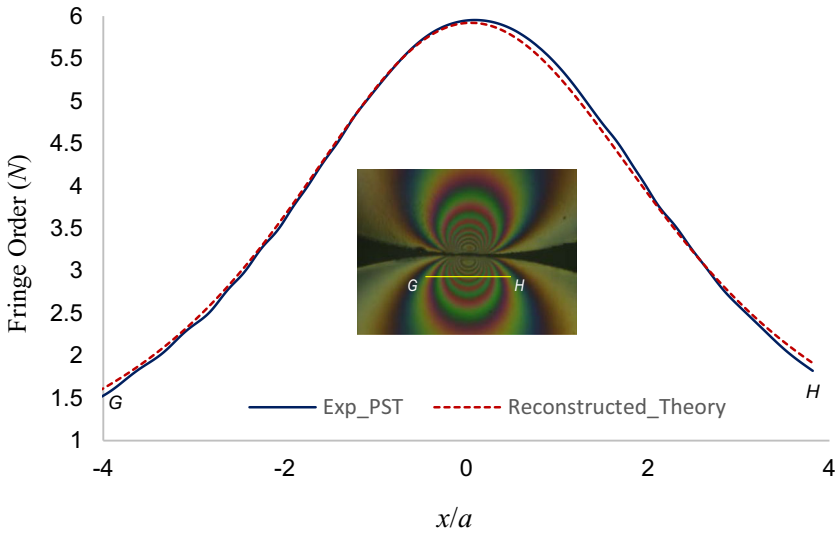

Fig. 13 Interface of two discs - variation in the fringe order along line *GH* (at $y = 2a$) obtained from PST and reconstructed from least squares results

Table 2 Comparison of contact zone parameters obtained for different contacting interfaces

Contacting Interface	Radius (mm)	Parameters obtained from nonlinear least squares result						Using Equations from Ref. [5]	
		From PST			From TFP				
		a (mm)	k	μ	a (mm)	k	μ	a (mm)	μ
Two discs	30	0.69	0.024	0.011	0.65	0.06	0.025	0.68	0.018
Plate - punch	2	5.72	0.958	0.075	5.65	0.953	0.034	–	–

To verify the generality of the equations proposed (equations (10)–(16)), the contacting situation of the two discs shown in Fig. 10(b) is also analyzed, where contact parameter a is 0.69 mm with $k = 0.024$ and $\mu = 0.013$. The isochromatics in the contact zone are reconstructed with the results obtained from the least squares analysis. Fringe orders at $y = 2a$ (line GH) from PST and the reconstructed contact zone are plotted in Fig. 13.

Similarly, the fringe order data obtained from TFP are also processed for both contact zones, and the results are comparable for both digital photoelastic methods (Table 2). The contact parameters obtained for the Hertzian contact zone are compared with the results obtained from contact field equations reported in the literature [5]. These results clearly show the generality of the proposed expressions. For non-conformal contacts, the value of k indicates that the complete contact length (b) is negligible in this case, and the proposed model (equations (10)–(16)) captures the Hertzian contact field [22, 23].

Conclusion

In this work, the application of digital photoelasticity to determine contact parameters in conformal contacts zones is established for the first time. In the initial part of this work, the explicit equations reported for a flat punch with rounded edges are generalized to represent both conformal and non-conformal (Hertzian) contact zones with an arbitrary radius of curvature of the contacting bodies. The set of generalized equations is verified by plotting simulated isochromatics for different contact parameters. A generic algorithm is developed to determine unknown contact parameters for conformal and non-conformal geometries from the whole-field isochromatic data using a nonlinear least squares method and is initially verified using theoretically generated isochromatic data.

For high-fringe gradients near the contact zones, the suitability of different digital photoelastic methods is discussed in detail. An improved four-step PST is proposed, allowing the evaluation of isochromatic and isoclinic data with the minimum number of images. This is mainly due to recent advancements making it possible to extract fringe order data from a single isochromatic image up to twelve fringes [11]. Isochromatic data for conformal and non-conformal contact zones are experimentally obtained and used in conjunction with the implemented non-linear least squares algorithms. For a flat punch with rounded edge contact, the value of k obtained from the nonlinear least squares ($k = 0.958$) is in the expected range of conformal contacts. When the contact model is switched to non-conformal geometry, the value of k is 0.024, which indicates a typical Hertzian contact.

Acknowledgements The authors would like to acknowledge partial support from the IITM-ISRO cell project (APM/14-15/154) for carrying out the research reported in this paper.

Appendix 1

Parameters u_1, u_2, u_3, u_6, v_1, and v_6 used in equations (10)–(15) are functions of x, y, a and b and are defined as

$$u_1(x,y) = \frac{\sqrt{2\sqrt{c_1} + 2c_2}}{2} \tag{A.1}$$

$$u_2(x,y) = \frac{\ln(\gamma_1)}{2} \tag{A.2}$$

$$u_3(x,y) = \frac{\ln(\gamma_2)}{2} \tag{A.3}$$

$$u_6(x,y) = \frac{x\left(x^2 + y^2 - a^2 + \sqrt{c_1}\right)}{\sqrt{2{c_1}^{1.5} + 2c_1c_2}} \tag{A.4}$$

$$v_1(x,y) = -\mathrm{sgn}(x)\frac{\sqrt{2\sqrt{c_1} - 2c_2}}{2} \tag{A.5}$$

$$v_2(x,y) = \theta_1 - \theta_2 \tag{A.6}$$

$$v_3(x,y) = \theta_3 - \theta_4 \tag{A.7}$$

$$v_6(x,y) = -\frac{y\left(x^2 + y^2 + a^2 - \sqrt{c_1}\right)}{\sqrt{2{c_1}^{1.5} + 2c_1c_2}} \tag{A.8}$$

The additional functions used in equations (A.1)–(A.8) are defined as

$$\gamma_1 = \frac{\sqrt{c_3} + c_5 + \sqrt{2c_5}\sqrt{\sqrt{c_3} + c_4}}{\sqrt{c_3} + c_5 - \sqrt{2c_5}\sqrt{\sqrt{c_3} + c_4}} \tag{A.9}$$

$$\gamma_2 = \frac{\sqrt{c_3} + 1/c_5 + \sqrt{2/c_5}\sqrt{\sqrt{c_3} + c_4}}{\sqrt{c_3} + 1/c_5 - \sqrt{2/c_5}\sqrt{\sqrt{c_3} + c_4}} \tag{A.10}$$

$$\theta_1 = \arcsin\left[\frac{\sqrt{2}}{2}\sqrt{\sqrt{c_3}-c_4}, \frac{\sqrt{2}}{2}\sqrt{\sqrt{c_3}+c_4}+\sqrt{c_5}\right] \quad \text{(A.11)}$$

$$\theta_2 = \arcsin\left[\frac{\sqrt{2}}{2}\sqrt{\sqrt{c_3}-c_4}, \frac{\sqrt{2}}{2}\sqrt{\sqrt{c_3}+c_4}-\sqrt{c_5}\right] \quad \text{(A.12)}$$

$$\theta_3 = \arcsin\left[\frac{\sqrt{2}}{2}\sqrt{\sqrt{c_3}-c_4}, \frac{\sqrt{2}}{2}\sqrt{\sqrt{c_3}+c_4}+\sqrt{1/c_5}\right] \quad \text{(A.13)}$$

$$\theta_4 = \arcsin\left[\frac{\sqrt{2}}{2}\sqrt{\sqrt{c_3}-c_4}, \frac{\sqrt{2}}{2}\sqrt{\sqrt{c_3}+c_4}-\sqrt{1/c_5}\right] \quad \text{(A.14)}$$

With the terms c_1,- c_5 defined as

$$c_1 = \left((a+x)^2+y^2\right)\left((a-x)^2+y^2\right) \quad \text{(A.15)}$$

$$c_2 = x^2-y^2-a^2 \quad \text{(A.16)}$$

$$c_3 = \frac{(a-x)^2+y^2}{(a+x)^2+y^2} \quad \text{(A.17)}$$

$$c_4 = \frac{a^2-x^2-y^2}{(a+x)^2+y^2} \quad \text{(A.18)}$$

$$c_5 = \frac{a-b}{a+b} \quad \text{(A.19)}$$

References

1. Johnson KL (2003) Contact mechanics. Cambridge University Press
2. Hills DA, Nowell D, Sackfield A (1993) Mechanics of elastic contacts, Butterworth Heinemann Ltd
3. Muskelishvili NL (1977) Some basic problems of the mathematical theory of elasticity. Fourth ed., Springer-Science Business Media 1977
4. Sackfield A, Mugadu A, Hills DA (2002) The influence of an edge radius on the local stress field at the edge of a complete fretting contact. Int J Solids Struct 39:4407–4420
5. Smith JO, Liu CK (1953) Stresses due to tangential and normal loads on an elastic solid with application to some contact stress problems. J Appl Mech 20:157–166
6. Ciavarella M, Hills DA, Monno G (1998) The influence of rounded edges on indentation by a flat punch. J Mech Eng Sci 212(Part C): 319–327
7. Vazquez J, Navarro C, Jaime D (2014) Explicit equations for the half-plane sub-surface stress field under a flat rounded contact. J Strain Anal 49(8):562–570
8. Ramesh K (2000) Digital photoelasticity: advanced techniques and applications. Springer-Verlag, Berlin, Heidelberg
9. Ramesh K (2015) Digital photoelasticity. In: Rastogi P (ed) Digital optical measurement techniques and applications. Artech House, London, UK, pp 289–344
10. Ramesh K, Gupta S, Kelkar AA (1997) Evaluation of stress field parameters in fracture mechanics by photoelasticity- revisited. Eng Fract Mech 9:189–210
11. Ramesh K, Ramakrishnan V, Ramya C (2015) New initiatives in single-colour image-based fringe order estimation in digital photoelasticity. J Strain Anal Engng Design September 2. doi: https://doi.org/10.1177/0309324715600044
12. Ramesh K, Kasimayan T, Neethi Simon B (2011) Digital photoelasticity – a comprehensive review. J Strain Anal Engng Design 46(1):245–266
13. Ramji M, Ramesh K (2010) Adaptive quality guided phase unwrapping algorithm for whole-field digital photoelastic parameter estimation. Strain 46(2):184–194
14. Petrucci G (1997) Full-field automatic evaluation of an isoclinic parameter in white light. Exp Mech 37(4):420–426
15. Brown GM, Sullivan JL (1990) The computer-aided holophotoelastic method. Exp Mech 30(2):135–144
16. Patterson EA, Wang ZF (1991) Towards full field automated photoelastic analysis of complex components. Strain 27(2):49–56
17. Ajovalasit A, Barone S, Petrucci G (1998) A method for reducing the influence of the quarterwave plate error in phase-shifting photoelasticity. J Strain Anal Engng Design 33(3):207–216
18. Ramesh K, Deshmukh SS (1997) Automation of white light photoelasticity by phase-shifting technique using colour image processing hardware. Opt Lasers Eng 28(1):47–60
19. Vivek R, Ramesh K (2017) Scanning schemes in white light photoelasticity – part II. novel fringe resolution guided scanning scheme. Opt Lasers Eng 92(1):141–149
20. Ramesh K, Hariprasad MP, Vivek R (2015) Robust multidirectional smoothing of isoclinic parameter in digital photoelasticity. Opt Eng 54(8):081205–081214
21. Hariprasad MP (2017) New initiatives in digital photoelastic parameter evaluation and its application to contact problems. Ph.D. Thesis, Indian Institute of Technology Madras
22. Hariprasad MP, Ramesh K (2018) Analysis of contact zones from whole field isochromatics using reflection photoelasticity. Opt Lasers Eng 105(1):86–92
23. Hariprasad MP, Ramesh K Evaluation of Hertzian contact parameters from whole field displacement data. J Strain Anal Eng Design 52(7):403–409